ACS OMEGA

http://pubs.acs.org/journal/acsodf

Article

Multi-objective Optimization and Control of Self-Heat Recuperative Azeoropic Distillation for Separating an Ethanol/Water Mixture

Lumin Li,* Na Yu, and Yi Zhu

Cite This: *ACS Omega* 2022, 7, 11382−11394

Read Online

ACCESS | Metrics & More | Article Recommendations

ABSTRACT: Azeotropic distillation is an important method for the separation of an ethanol/water mixture, while the main disadvantage of azeotropic distillation is its high energy consumption. Since the self-heat recuperation technology can effectively recover and utilize the heat of effluent stream in thermal processes, it is introduced into the ethanol dehydration process. The conventional azeotropic distillation and self-heat recuperative azeotropic distillation (SHRAD) are simulated and optimized with multiple objectives. There exists a design point in the Pareto solution set for which the total annual cost is the lowest, the thermodynamic efficiency is the highest, and the CO_2 emission is the least. Based on the specified design, the dynamic characteristics of the SHRAD configuration are studied, and two control structures are proposed. The improved control structure of the SHRAD process works well under the feed flowrate and composition disturbance, and the SHRAD system can obtain a high-purity ethanol product. The results show that the SHRAD process has significant advantages over conventional azeotropic distillation in terms of economic and environmental benefits. In addition, an effective control structure can ensure the stable operation of the SHRAD process.

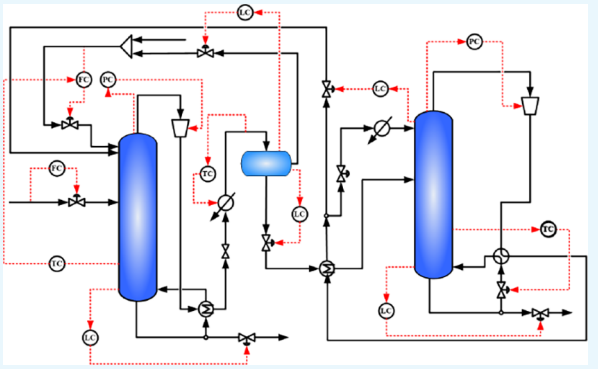

1. INTRODUCTION

With the decline of fossil fuels, renewable energy has attracted a lot of research. Bioethanol is a promising alternative energy source in the short and medium term.[1] In addition, bioethanol is easier to mix with gasoline than with other alternative fuels. The dehydration process is one of the key technologies in ethanol production since the ethanol content obtained from biomass production is low.[2] The dehydration process mainly includes two steps, which are both of high energy consumption. The mass fraction of ethanol obtained from the ordinary distillation section can reach 92.4− 94 wt %. At this time, ethanol and water will form azeotrope, which is difficult to be further purified by ordinary distillation, and thus other dehydration methods need to be used.[3,4] Azeotropic distillation,[5,6] extractive distillation,[7,8] and pressure-swing distillation[9] are all effective methods for separating azeotropic mixtures, and lots of energy-saving technologies are proposed to improve these processes.[10,11]

The introduction of process intensification and integration technology in distillation can effectively reduce the energy consumption and improve the energy efficiency, such as heat-integrated distillation,[12,13] dividing-wall column distillation,[14,15] and cyclic distillation.[16] In recent years, the self-heat recuperation technology for low-temperature heat source recovery has received wide attention,[17,18] which can be used for the distillation process to further reduce the energy consumption. It takes advantage of the heat exchange between the import and export streams that realizes the energy recovery. Kansha et al.[19,20] applied the self-heat recuperation distillation (SHRD) in cryogenic air separation and crude distillation, and the results showed that the energy saved could reach 36 and 52%, respectively. Long and Lee[21] applied the self-heat recuperative technology to natural gas liquid recovery, and the total annual cost (TAC) of the SHRD process could save more than 40% when compared with conventional distillation.

Although the SHRD process has a significant energy-saving effect in the steady-state simulation, very few investigations of process control for this self-heat recuperative process have been performed. Therefore, in order to apply this technology to the industrial processes, it is necessary to design an operation system with investigation of their process optimization and control. Compared with conventional distillation, the structure of SHRD is more complex and the

Received: January 24, 2022
Accepted: March 15, 2022
Published: March 22, 2022

process optimization is more complicated. The process optimization of the SHRD is a highly nonlinear multi-objective optimization problem. Since the multi-objective optimization technique has more advantages than single-objective optimization, especially when conducting the heat-integrated distillation system with compressors,[22] this paper will use the multi-objective genetic algorithm to optimize the SHRD process of ethanol dehydration. The conventional azeotropic distillation (CAD) and self-heat recuperative azeotropic distillation (SHRAD) are proposed to separate the ethanol/water mixture, and their performances are discussed. In addition, understanding the dynamic characteristics and establishing an effective control structure are very important to apply and expand this SHRAD to the industrial processes. It is necessary to design an SHRAD system with investigation of its dynamics. Compared with conventional azeotropic distillation, the process control of SHRAD configuration is more complicated due to its high thermal integration degree and the mutual influence of various variables in the distillation column. Although a few articles on SHRD have been published, the control of SHRAD has received little attention, and few articles on these areas could be found in the open literature. Therefore, the process control of the SHRAD process is investigated in order to obtain an effective control scheme.

The purpose of this paper is to explore the optimum flowsheet and process control of the SHRAD process for ethanol dehydration. In this paper, the steady-state simulation, optimization, and process control of the SHRAD for ethanol/water systems were carried out, which can enrich the theoretical study of the SHRD process. The multi-objective genetic algorithm is used to optimize the SHRAD process. The dynamic control of the SHRAD process is studied, and the effective control structure is proposed. It can be useful in promoting the availability of bioethanol to the society.

2. MATERIALS AND METHODS

2.1. Steady-State Simulation. *2.1.1. Steady-State Simulation of Conventional Azeotropic Distillation.* The entrainer for separating an ethanol/water mixture should meet the general screening principle of azeotrope. Benzene,[23−25] *n*-pentane,[26] cyclohexane,[27,28] and isooctane[29] are usually adopted as the entrainer, among which benzene and cyclohexane are widely used. It must be pointed out that benzene can easily enter into the atmosphere and additional energy is needed for recycling. In addition, benzene has a negative environmental impact due to toxicity issues. Herein, we choose benzene as the entrainer, mainly because our investigation is based on the research of Kansha et al.,[30] in which they proposed the SHRD process and adopted benzene as the entrainer for ethanol dehydration. In this paper, the feed conditions are a flow rate of 100 kmol/h, a composition of 85.0/15.0 mol % ethanol/water, and a temperature of 77.0 °C. The two product specifications are set to be as follows: the ethanol product has a purity of 99.9 mol %, and the ethanol impurity in the water product is not more than 0.8 mol %. The UNIQUAC model is adopted to describe the non-ideal gas−liquid behavior of the ethanol/water/benzene system, and Table 1 shows the binary interactive parameters of the UNIQUAC model.

Figure 1 shows the flowsheet of conventional azeotropic distillation for ethanol/water mixture separation, which includes the azeotropic distillation column (C1) and benzene recovery column (C2). In the azeotropic distillation column, there are two recycled streams, namely, the organic-phase stream separated from the decanter and the product from the top of column C2.

Table 1. Binary Interactive Parameters of the UNIQUAC Model

component *i*	ethanol	ethanol	water
component *j*	water	benzene	benzene
unit	°C	°C	°C
A_{ij}	2.0046	−0.0464	0
A_{ji}	−2.4936	0.4665	0
B_{ij}	−728.9705	76.5759	−369.01
B_{ji}	756.9477	−556.4752	−860.81

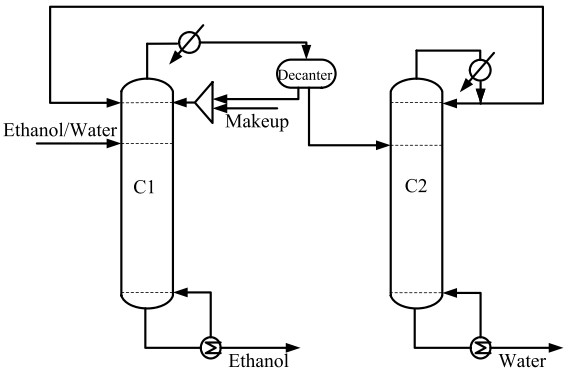

Figure 1. Flowsheet of the conventional azeotropic distillation process.

As shown in Figure 1, the column C1 is simulated by the combination of stripper, decanter, and heat exchanger models, and the column C2 is simulated by the Radfrac model in Aspen Plus. The liquid ethanol/water mixture is fed into column C1. The stages of column C1 are set at 30. The organic phase separated from the decanter and the distillate of column C2 is recycled to the top of column C1 to provide the entrainer. The fresh mixture enters the third stage. The pressure of the azeotropic distillation column is set to 2 atm because a control valve on the overhead vapor line is needed. A 99.9 mol % ethanol is obtained from the bottom of column C1 (99.6 °C), and the steam from the top of C1 (84.6 °C) was decompressed into the cooler for cooling to 40.0 °C, which then entered the decanter. Since there was a small amount of benzene loss in both products, a small amount of liquid benzene at 25 °C was added and mixed with the reflux organic phase. The number of stages for column C2 is 16. The water phase separated from the decanter enters the fourth stage of column C2, and 99.26 mol % water was obtained from the bottom of column C2.

2.1.2. Steady-State Simulation of the SHRAD Process. In the conventional azeotropic distillation process, the temperature difference between the top and bottom of column C1 is 15 °C, and the temperature difference between the top (66.0 °C) and bottom (101.0 °C) of column C2 is 35 °C. Therefore, the top steam from both C1 and C2 can be recycled as a low-temperature heat source. In the work of Kansha et al.,[30] they applied three individual compressors for the individual heat integration of the columns and the intermediate preheater. However, the introduction of three compressors makes the design and operation of such distillation columns more complicated, also resulting in a significant capital cost increase, as compared to a conventional distillation process. Therefore,

https://doi.org/10.1021/acsomega.2c00478
ACS Omega 2022, 7, 11382−11394

considering the economical benefit and structural simplicity of the azeotropic distillation system, the SHRAD design is proposed in our study, which not only aims to reduce the energy consumption of the reboiler but also takes into account the preheating of the feed to further reduce the operating cost.

Figure 2 shows the flowsheet of the SHRAD process. Compared with the conventional azeotropic distillation process, two compressors ($Comp_1$ and $Comp_2$) are introduced into this process. The feed and product conditions of the SHRAD process in Figure 2 are consistent with the traditional azeotropic process. Before entering the decanter, the top steam of column C1 (83.8 °C) is first compressed adiabatically by the compressor and then exchanged heat with the bottom steam of C1. After the heat exchange, the stream decompresses and is cooled before entering the decanter. The organic phase separated from the decanter and supplementary benzene were mixed and circulated to the first stage of C1. The aqueous phase from the decanter is heated into C2 as the feed stream. The top steam of C2 (77.0 °C) is compressed and used as the heat source for the reboiler of C2. After that, the stream still has a high temperature, and it is used to further heat the feed of C2. Finally, the stream is divided and recycled to C1 and C2.

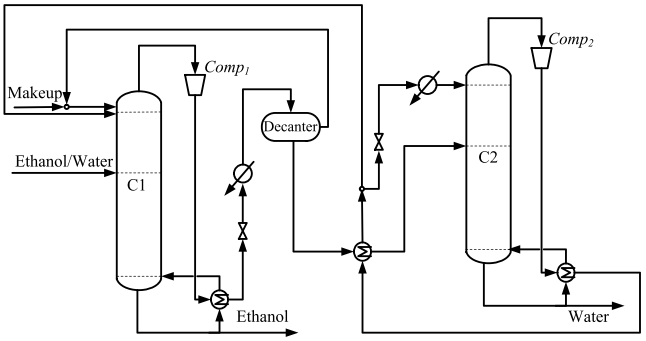

Figure 2. Flowsheet of the SHRAD process.

.

2.2. Optimization. The genetic algorithm is a stochastic search method based on the evolutionary law of the genetic mechanism of survival of the fittest in biology. The multi-objective genetic algorithm has been widely used in the optimization process of distillation systems.[31,32] The optimization of the SHRAD process is a mathematical problem of multi-objective optimization with complex calculation and high non-linearity. Alcántara-Avila et al.[22] used the multi-objective optimization technology to optimize the compressor-aided distillation sequences with heat integration, which provided a new idea for the optimization of the SHRAD process. In this section, the multi-objective genetic algorithm is used to optimize the SHRAD process. For comparison, the conventional azeotropic distillation and SHRAD processes were optimized by the multi-objective genetic algorithm.

TAC is an important index to evaluate the economic performance of chemical processes.[33] Douglas proposed the calculation method of the TAC in his book.[34] The TAC includes two parts, namely, the operating cost (OC) and the capital investment (CI). The TAC can be calculated as follows:

$$\mathrm{TAC(\$/year)} = \mathrm{OC} + \mathrm{CI}/T \tag{1}$$

Here, the operating cost is the energy cost, mainly including the utility cost such as steam, cooling water, and electricity, etc.. Capital investment mainly includes the column shell, tray, heat exchanger, compressor, and so on. T is the payback period. In this study, it was assumed that the capital payback period is 8 years and the operating time is 8000 h/year. Table 2 gives the relevant prices.

Table 2. Relevant Prices for the TAC Calculation

items	prices
utility	
low pressure steam (160 °C, 5 barg)	7.78 $/GJ
cooling water	0.354 $/GJ
electricity	6.9 $/GJ
entrainer	
benzene	13.22 $/kg

Seader et al.[35] proposed the thermodynamic efficiency η, which can be used to evaluate the energy economy of distillation systems. The thermodynamic efficiency can be expressed in eq 2:

$$\eta = \frac{W_{\min}}{\mathrm{LW} + W_{\min}} \tag{2}$$

where $W_{\min}$ (kJ/h) and LW (kJ/h) are the minimum separation work and loss work, respectively, and $W_{\min}$ can be expressed as follows:

$$W_{\min} = \sum_{\text{out of system}} nb - \sum_{\text{in to system}} nb \tag{3}$$

where n is the molar flow rate; b is the exergy, defined as $b = H - T_0S$, where H (kJ/kmol) is the molar enthalpy; S is the molar entropy, and T_0 (K) is the ambient temperature.

E_x (kW) is the exergy consumption by the system, which can be expressed as follows:

$$\begin{aligned} E_x &= W_{\min} + \mathrm{LW} \\ &= \sum_{\text{in to system}} Q_{\mathrm{R}}\left(1 - \frac{T_0}{T_{\mathrm{R}}}\right) - \sum_{\text{out of system}} Q_{\mathrm{C}}\left(1 - \frac{T_0}{T_{\mathrm{C}}}\right) \\ &\quad + W_s \end{aligned} \tag{4}$$

Here, Q_{R} (kW) and T_{R} (K) are the reboiler duty and reboiler temperature, respectively; Q_{C} (kW) and T_{C} (K) are the condenser duty and condenser temperature, respectively; and W_s (kW) is the shaft power.

Distillation is an extremely energy-consuming process, which comes with a large amount of carbon dioxide (CO_2) emissions. Therefore, the energy saving of the distillation process can reduce not only the steam cost but also the emission of greenhouse gases. From the perspective of fuel combustion, CO_2 emissions are generated as follows:

$$\mathrm{C}_x\mathrm{H}_y + \left(x + \frac{y}{4}\right)\mathrm{O}_2 \rightarrow x\mathrm{CO}_2 + \frac{y}{2}\mathrm{H}_2\mathrm{O} \tag{5}$$

Here, oxygen is excessive to ensure the complete combustion of fuel. x and y are the numbers of carbon and hydrogen atoms in fuel composition, respectively, and CO_2 emissions (kg/s) can be expressed as follows:[36,37]

https://doi.org/10.1021/acsomega.2c00478
ACS Omega 2022, 7, 11382−11394

$$P_{CO_2} = \left(\frac{Q_{Fuel}}{NHV}\right)\left(\frac{C\%}{100}\right)\alpha \quad (6)$$

Here, Q_{Fuel} (kW) is the amount of fuel burnt. NHV (kJ/kg) is the net heating value of fuel containing carbon C%. α (=3.67) is the molar mass ratio of carbon dioxide to carbon atoms. CO_2 emissions are closely related to the type of fuel used for heating. In this paper, coal was selected as the fuel, and NHV and C% were 22,000 kI/kg and 0.68 kg/kg, respectively. Q_{Fuel} is related to the energy consumption of process Q_{Proc} (kW), which can be expressed as follows:

$$Q_{Fuel} = \frac{Q_{Proc}}{\eta_{Furn}} \quad (7)$$

Here, η_{Furn} is the heating efficiency of the boiler, and it can be calculated with an empirical value of 0.8−0.9.

2.2.1. Optimization of the Conventional Azeotropic Distillation Process. In the conventional azeotropic distillation process, the number of stages and the reboiler duty have a great influence on its economy. There is a competitive relationship between the number of stages and the energy consumption of the reboiler. Therefore, the optimization objective of the conventional azeotropic distillation process is defined as the number of stages N_i and the reboiler duty Q_i, which are in competition and are constrained by the desired purity and recovery of a product. Hence, the optimization problem of the conventional azeotropic distillation can be described as follows:

$$\min(N_i, Q_i) = f(R_2, N_i, N_{F,i}, F_{EN}, F_{PE})$$
$$s.\ t.$$
$$\vec{y}_k \geq \vec{x}_k \quad (8)$$

Here, the subscript i = 1 is the azeotropic distillation column and i = 2 is the benzene recovery column, R_2 is the reflux ratio of a benzene recovery column, $N_{F,i}$ is the feed location of column i, F_{EN} is the flow rate of the entrainer, F_{PE} is the flow rate of product ethanol, and $\vec{y}_k$ and $\vec{x}_k$ are the vectors of the obtained and required purity and recovery for a specified product, respectively. Table 3 presents the optimization ranges

Table 3. Optimization Ranges of the Design Variables in the CAD Process

design variables	variable ranges
reflux ratio R_2	[0.1, 0.3]
number of stages N_1	[28, 35]
number of stages N_2	[10, 25]
feeding location $N_{F,1}$	[2, 18]
feeding location $N_{F,2}$	[2, 12]
ethanol flowrate F_{PE} (kmol/h)	[84, 86]
entrainer flowrate F_{EN} (kmol/h)	[105, 120]

of the design variable in the CAD process. For the CAD process, 2000 individuals and 40 generations were used as the optimization parameters, and the crossover operator and variation fraction were set at 0.80 and 0.05, respectively.

2.2.2. Optimization of the SHRAD Process. In the SHRAD process, the number of stages has a great influence on the equipment investment. In addition, the energy consumption of compressors also plays a decisive role in the operation cost. However, the number of stages has a competitive relationship with the energy consumption of compressors. For the optimization of the SHRAD process, the objective function is defined as the number of stages and the compressor power. The constraint conditions are the purity and recovery of ethanol. Therefore, the optimization of the SHRAD process is a problem aiming at obtaining the minimum N_i and W_i, which can be described as follows:

$$\min(N_i, W_i) = f(C_i, N_i, N_{F,i}, L_{SP,i}, V_{SP}, F_{EN})$$
$$s.\ t.$$
$$\vec{y}_k \geq \vec{x}_k \quad (9)$$

Here, N_i is the number of stages, W_i is the power of compressors, C_i is the compression ratio of the compressor, $N_{F,i}$ is the feed location, $L_{SP,i}$ is the ratio of the bottom product flow to the bottom liquid flow of a column, V_{SP} is the ratio of the recycled flow rate to the top steam of the recovery column, F_{EN} is the flow rate of the entrainer, $\vec{x}_k$ is the purity or recovery of the specified product, and $\vec{y}_k$ is the purity or recovery of the product obtained during the optimization process.

The optimization objectives of this SHRAD process include the number of stages in the azeotropic distillation column, the number of stages in the benzene recovery column, and the power of compressors. There is a mutual restriction and competition between the objectives, and the multi-objective optimization method is adopted for simultaneous optimization. Table 4 shows the optimization ranges for the design variables

Table 4. Optimization Ranges of the Design Variables

design variables	variable ranges
number of stages N_1	[27, 31]
number of stages N_2	[9, 16]
compression ratio C_1	[4.2, 6]
compression ratio C_2	[3.8, 4.1]
feeding location $N_{F,1}$	[2, 11]
feeding location $N_{F,2}$	[2, 8]
separation ratio $L_{SP,1}$	[0.10, 0.15]
separation ratio $L_{SP,2}$	[0.05, 0.06]
separation ratio V_{SP}	[0.14, 0.16]
entrainer flowrate F_{EN} (kmol/h)	[110, 150]

of the SHRAD process. For the SHRAD process, the multi-objective optimization parameters are set the same as those of the conventional azeotropic distillation.

2.3. Dynamic Control. Although the SHRD process can significantly reduce the energy consumption, its research is mainly based on the steady-state design. Understanding the dynamic characteristics of the SHRAD system and establishing an effective control structure are very important in promoting the application. Compared with the conventional azeotropic distillation, the control of the SHRAD process is more complicated due to its thermal integration configuration and the mutual influence of various variables. Therefore, the dynamic characteristic analysis of the SHRAD process was carried out in order to obtain the effective control scheme.

The tray-sizing option in Aspen Plus is adopted to calculate the needed size of equipment, such as column diameter. The base and reflux drum volumes are set to maintain 10 min holdup with 50% liquid level. Pumps and valves are almost specified to provide pressure drops of about 3 atm with the valve half open. Some necessary compressors, pumps, and valves are added to the steady-state of the SHRAD process,

https://doi.org/10.1021/acsomega.2c00478
ACS Omega 2022, 7, 11382−11394

and then pressure-driven simulation in Aspen Dynamics is used to investigate the dynamic control of the SHRAD process. When establishing the control structure, the normal settings of the proportional-integral (PI)-type power-flow controller are K_C = 0.5 and τ_I = 0.3 min. The level loops are P-only and the K_C is 2, and the pressure controller is PI with its default values. Considering measurement and actuator lags in any real physical system, a 1 min dead time is inserted into the temperature control loops. Refer to Luyben's book for the detailed tuning and setting process.[38]

3. RESULTS AND DISCUSSION

3.1. Optimization Results. *3.1.1. Optimization Results of the SHRAD Process.* The Pareto solution set of the SHRAD process is given in Figure 3, and it satisfies the constraints of product purity and recovery, which includes all design points from the minimum number of stages to the minimum compression power.

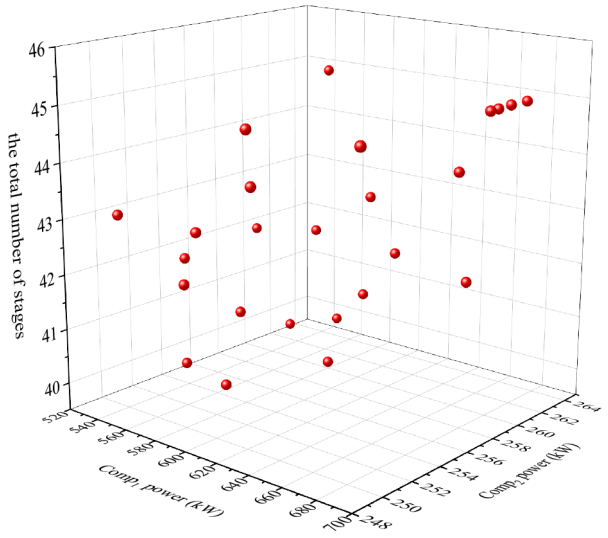

Figure 3. Pareto solution set of the SHRAD process for an ethanol/water mixture.

Figure 4 shows the influence of different numbers of stages on the total power of compressors in the SHRAD process. It can be seen from Figure 4 that, with the changes in the number of stages, the total power of compressors fluctuates within a certain range, resulting in a high energy consumption section and low energy consumption section. The SHRAD system under different design variables can achieve the same energy consumption, and the lower energy consumption of compressors has more advantages.

Figure 5 shows the relationship between the number of stages and the feed location. As shown in Figure 5, under the condition of satisfying product purity and recovery, the feed location was mainly stable near the fourth stage with the change in the number of stages in the azeotropic distillation column. When the number of stages in the recovery column changed, the feed location was mainly stable near the sixth stage. Thus, the feed location was relatively stable when the number of stages changed.

The TAC of the SHRAD process was calculated based on the Pareto solution set. Figure 6 shows the relationship between the compression ratio of two compressors and the TAC of the SHRAD process. As shown in Figure 6, the TAC

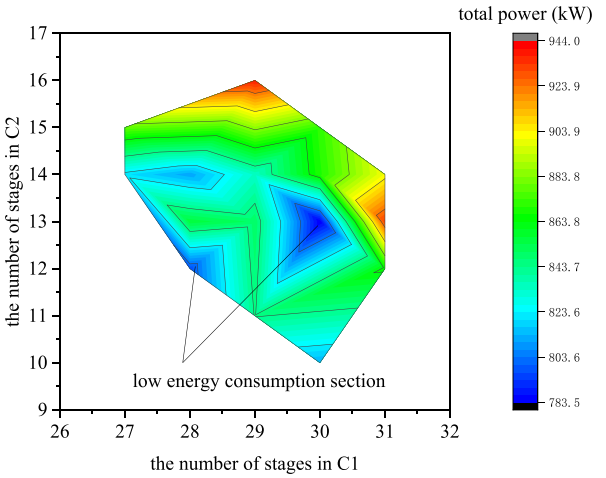

Figure 4. Effects of the number of stages in the azeotropic distillation column (C1) and benzene recovery column (C2) on the total compressor power.

of the SHRAD system increased rapidly when the compression ratio of compressor $Comp_1$ increased. The TAC changed steadily when the compression ratio of compressor $Comp_2$ changed. Therefore, the compressor $Comp_1$ operating at a low compression ratio is more advantageous. In addition, when there is a competitive relationship between the number of stages and the compression ratio of compressor $Comp_2$, the influence of the number of stages on the TAC should be mainly considered, and the feasible solution with a lower number of stages should be selected.

Three commonly used evaluation indexes, the TAC, thermodynamic efficiency (η), and CO_2 emissions (P_{CO2}), are used for the economic and environmental performance of the SHRAD process. Figure 7 shows the relationship among the evaluation indexes at each design point of the Pareto solution set for the SHRAD process. When the TAC of the system is low, the carbon dioxide emission is also low, the thermodynamic efficiency is high, and the distribution of each design point is concentrated along the diagonal, which also shows the relative relationship among the three performance evaluation indexes.

3.1.2. Performance Evaluation and Comparison. According to the calculation results of the TAC, thermodynamic efficiency, and CO_2 emissions, as shown in Figure 7, there is a proper design point in the Pareto solution set. For this design point of the SHRAD process, the thermodynamic efficiency is the highest and the TAC and the carbon dioxide emissions is the lowest. The parameters and mass balance of the CAD and SHRAD processes at the specified design point are presented in Table 5 and Table 6, respectively.

Table 7 lists the detailed cost distribution of the CAD and SHRAD processes. As shown in Table 7, when compared with conventional azeotropic distillation (CAD), the TAC of the SHRAD is increased by 12% with a payback period of 3 years. When the payback periods are 5 years and 8 years, the TAC of the SHRAD can be saved by about 28.02% and 39.55%, respectively. Thus, it can be seen that with increasing the capital payback period, more TAC will be saved by the SHRAD process. This is mainly because the capital investment costs are significantly increased by applying the compressors to the distillation system. However, great energy savings can be achieved by using the self-heat recuperation technology, which

https://doi.org/10.1021/acsomega.2c00478
ACS Omega 2022, 7, 11382−11394

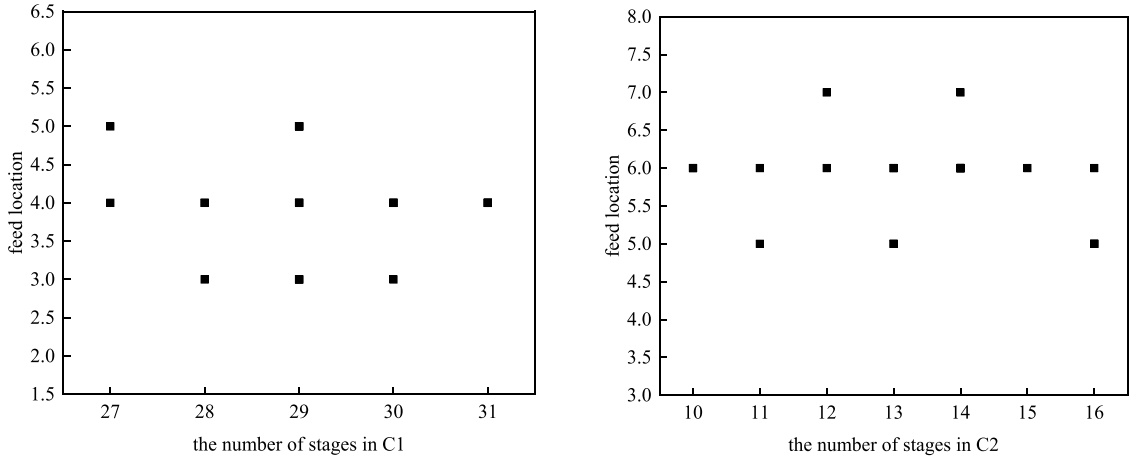

Figure 5. Relationship between the number of stages and feed locations.

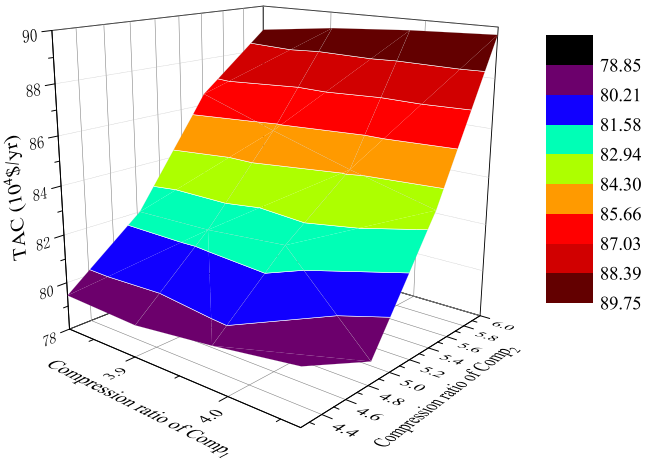

Figure 6. Effects of the compression ratios on the TAC of the SHRAD process.

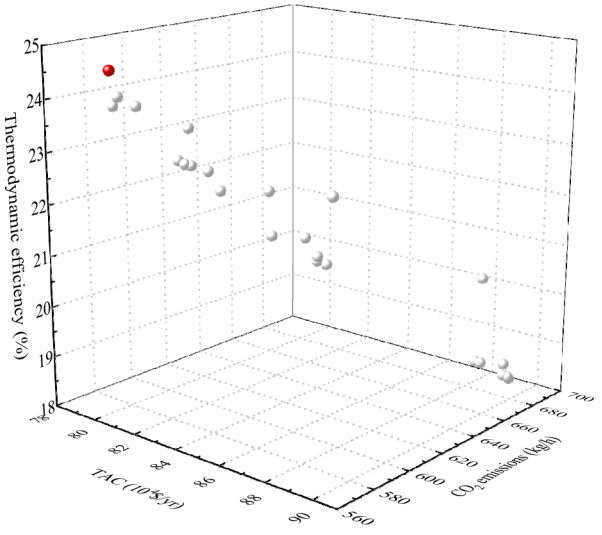

Figure 7. Relationship among the TAC, thermodynamic efficiency, and CO_2 emissions of the Pareto front in the SHRAD process.

can compensate the adverse effects caused by the increased investment costs. Therefore, the SHRAD design can be considered for better economical benefit in the long run.

Table 5. Parameters of the CAD and SHRAD Processes

	CAD process		SHRAD process	
parameter	C1	C2	C1	C2
operating pressure (atm)	2	1	2	1
top temperature (°C)	84.6	66.0	83.8	77.0
bottom temperature (°C)	99.6	101.1	99.5	100.3
reflux ratio	0.966	0.116	1.065	0.168
number of stages	28	17	30	13
feed location	8	9	4	6
feeding location of entrainer	1		1	
feeding location of recycled stream	1		1	
condenser duty (kW)	−3192.96	−1572.54	−2078.34	−488.13
reboiler duty (kW)	3151.53	1720.98	3044.37	279.76
preheat heat transfer (kW)				1457.10
compressor power (kW)		-	533.73	250.18
ethanol/water purity (mol %)	99.90	99.26	99.91	99.31

Table 8 summarizes the thermodynamic efficiency and CO_2 emission of the CAD and SHRAD processes at the specified design point. According to Table 8, the thermodynamic efficiency and CO_2 emission of the SHRAD process are 24.56% and 567.53 kg/h, respectively. When compared with the CAD process, the lost work and the CO_2 emission of the SHRAD process decreased by 49.63 and 51.73%, respectively. It indicated that the introduction of self-heat recuperation technology has significant economic and environmental benefits to the CAD process.

3.2. Dynamic Control. *3.2.1. Dynamic Characteristics of the SHRAD Process.* In the dynamic model of the SHRAD system, the operation pressure is controlled by the compressor, and then the feed flowrate and feed composition disturbances are introduced to analyze the dynamic characteristics of the SHRAD system. Figure 8 shows the dynamic responses of product purity after introducing the feed flowrate disturbances to the SHRAD system. As shown in Figure 8, when the feed flow increased by 10%, the ethanol purity decreased and stabilized around the 6th hour, and it was below the set value of 99.86 wt %. The purity of water increases with the increase in the feed flowrate and reaches a stable value around the 4th hour. When the feed flow decreased by 10%, the purity of ethanol decreased significantly, then increased gradually, and

https://doi.org/10.1021/acsomega.2c00478
ACS Omega 2022, 7, 11382−11394

Table 6. Mass Balance for the Optimized CAD and SHRAD Processes

		input stream		output stream	
	units	ethanol/water	makeup	ethanol	water
CAD process					
ethanol	mol/mol	0.85	0	0.9990	0.0074
water	mol/mol	0.15	0	0.0002	0.9926
benzene	mol/mol	0	1	0.0008	trace
overall amount	kmol/h	100	0.07	84.9841	15.0859
SHRAD process					
ethanol	mol/mol	0.85	0	0.9991	0.0069
water	mol/mol	0.15	0	0.0001	0.9931
benzene	mol/mol	0	1	0.0008	trace
overall amount	kmol/h	100	0.07	84.9728	15.0973

Table 7. Cost Distribution of the Traditional Azeotropic Distillation and SHRAD Process

	CAD process	SHRAD process
installed column shells cost ($10^3$$)	816.68	765.92
installed column trays cost ($10^3$$)	22.11	20.55
installed reboilers/heat exchangers cost ($10^3$$)	419.71	585.53
installed condenser/cooler cost ($10^3$$)	504.66	158.21
installed compressor cost ($10^3$$)		1759.08
total capital cost ($10^3$$)	1763.16	3289.29
steam cost ($10^3$$/year)	1083.13	
cooling water cost ($10^3$$/year)	10.42	1.58
electricity cost ($10^3$$/year)		381.54
total operating cost ($10^3$$/year)	1093.55	383.12
TAC with a capital payback period of 3 years ($10^3$$/year)	1681.27 (0%)	1479.55(12.0%)
TAC with a capital payback period of 5 years ($10^3$$/year)	1446.182 (0%)	1040.978 (28.02%)
TAC with a capital payback period of 8 years ($10^3$$/year)	1313.95 (0%)	794.28 (39.55%)

Table 8. Performance Indexes of the CAD and SHRAD Processes

	CAD process	SHRAD process
minimum work of separation (kW)	36.44	36.44
lost work (kW)	222.19 (0%)	111.92 (−49.63%)
thermodynamic efficiency (%)	14.09	24.56
CO_2 emission (kg/h)	1175.85 (0%)	567.53 (−51.73%)

finally stabilized at about the ninth hour and returned to the initial purity. The purity of water began to stabilize above the set value of 98.25 wt % after experiencing two large fluctuations. When the flowrate changes by 20%, the fluctuation of the two products is basically the same as that of the flowrate change by 10%. However, as can be seen from Figure 8, the higher the increase in the flow, the longer the stability time of the product will be and the lower the purity of the product will be. It indicates that the greater the change in the feed flowrate, the more serious the impact on the product will be. The decrease in feed flow mainly affects the overshoot and stability time of the product, especially the ethanol product, which is an unfavorable factor for the system.

Figure 9 shows the dynamic responses of product purity after introducing the water composition disturbances to the SHRAD system. As can be seen from Figure 9, when the water composition increases by 10%, the purities of ethanol and water change slightly. When the water composition increases by 20%, the overshoot of product fluctuation is larger, the stability time is longer, and the ethanol purity no longer meets the set value. When the water composition is reduced by 10%, the ethanol purity drops sharply and then rises near the set value. However, when the water composition is reduced by 20%, the variation trend of the ethanol product is the same as that of 10%, but the overshoot is larger, and the lowest point is below 90.0 wt %. The change in water composition has little effect on the purity of the water product, and it can be stabilized at the set value after disturbances.

As shown in Figures 8 and 9, when the feed flow increased, the purity of the ethanol product could not meet the requirements. When the feed composition increased, the purity of ethanol and water could not meet the requirements. The feed flowrate and composition disturbances usually cause product purity fluctuation and produce a large overshoot, which makes the restoration to the set value difficult. Therefore, it is necessary to establish an effective control structure to the SHRAD system to ensure the product quality.

3.2.2. Control Strategy of the SHRAD Process. Figure 10 shows the temperature profile of the optimized SHRAD process. It can be seen from Figure 10 that the temperature slope at the 25th stage of the azeotropic distillation column is the largest, and thus it can be selected as the temperature-sensitive stage based on the slope criterion.[38] The 12th stage in the benzene recovery column has the largest temperature slope, while it is close to the column bottom, and the 11th stage with a relatively large slope is selected as the temperature-sensitive stage.

In the initial control structure of the SHRAD process, the liquid level control is first added to refer to the experience on conventional azeotropic distillation.[39] It is very important to control the total amount of liquid phases in the decanter. It is difficult to control the organic phase level by adjusting the flowrate of supplementary benzene because the amount of azeotrope is too small. It is found that the organic phase flow from the decanter can control its liquid level well, and the water phase level in the decanter is controlled by the feed flow of the benzene recovery column. The bottom liquid level of the azeotropic distillation column is controlled by the bottom product flowrate, and the top liquid level of the benzene recovery column is controlled by the top product flow rate. The bottom liquid level of the benzene recovery column is controlled by the bottom product flow rate. The flowrate of the feed mixture and the reflux flow of the organic phase are controlled by their valves, respectively, and the proportional control of the two streams is added to control the 25th stage temperature of the azeotropic distillation column (K_C = 1.45,

https://doi.org/10.1021/acsomega.2c00478
ACS Omega 2022, 7, 11382−11394

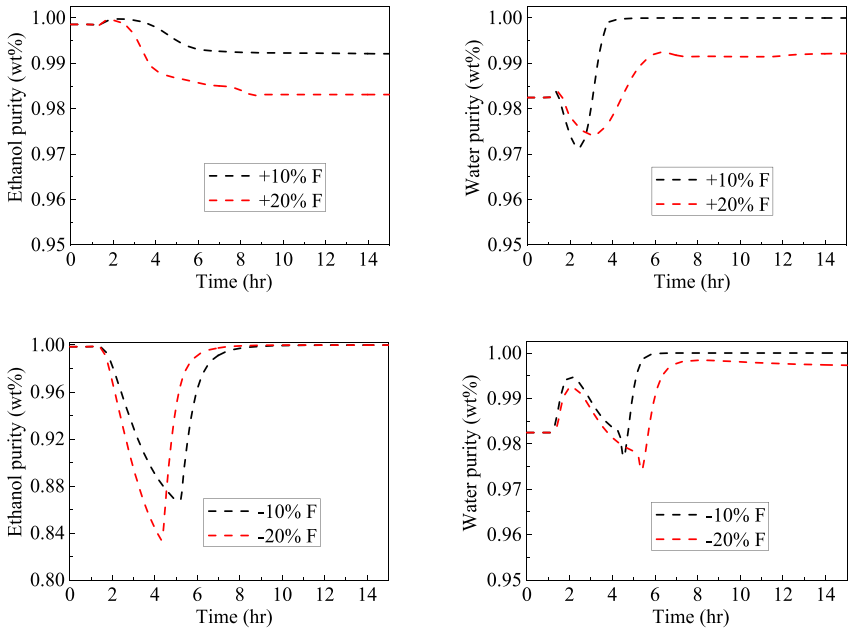

Figure 8. Dynamic responses of ethanol and water products when the feed flowrate changed by 10 and 20%.

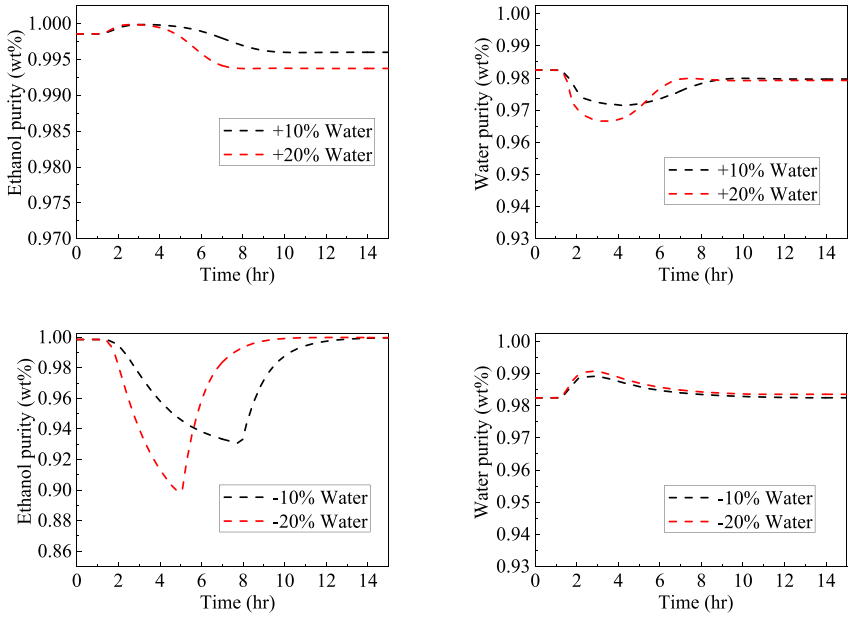

Figure 9. Dynamic responses of ethanol and water products when the water composition changed by 10 and 20%.

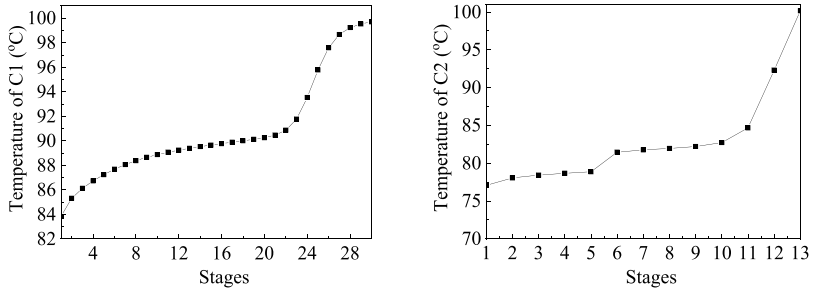

Figure 10. Temperature profile of the SHRAD process.

τ_1 = 18.46 min). The heat removed from the cooler is adjusted to control the temperature of flow feeding into the decanter. Since the bottom reboiler heat of the benzene recovery column is provided by its top steam, it cannot be used as a control variable. When controlling the azeotropic dividing-wall column with vapor recompression, Luyben[40] used the top steam flow

https://doi.org/10.1021/acsomega.2c00478
ACS Omega 2022, 7, 11382−11394

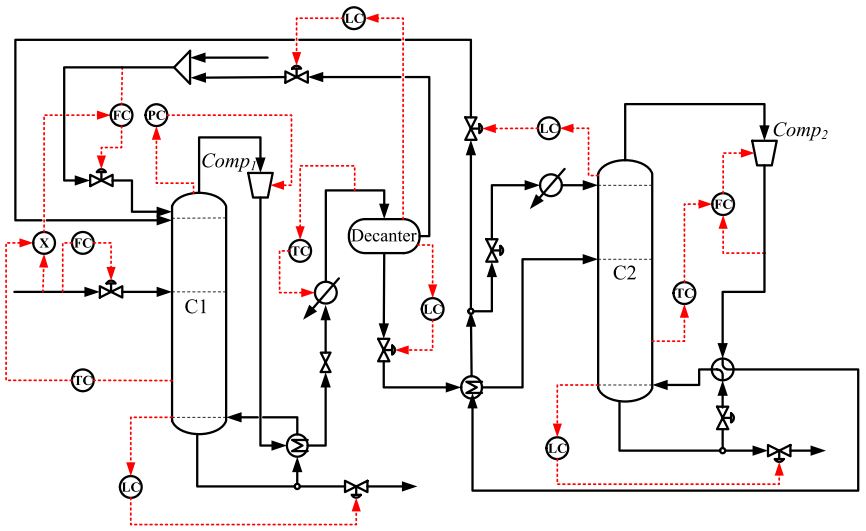

Figure 11. Initial control structure of the SHRAD process.

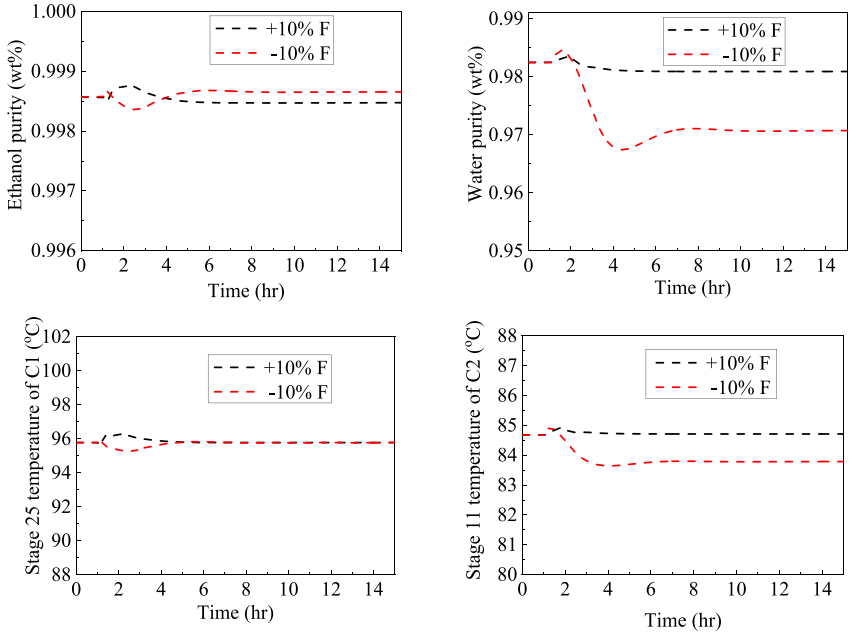

Figure 12. Dynamic responses of the initial control structure in ±10% feed flowrate changes.

of the column to control the stage temperature and used the compressor power to regulate the top steam flow. Therefore, the flowrate of top steam is used as the control variable to adjust the temperature of the 11th sensitive stage (K_C = 0.82, τ_I = 10.63 min). The compressor $Comp_2$ is used to adjust the top steam flowrate of the benzene recovery column. The corresponding control structure is shown in Figure 11.

Feed flow and composition disturbances are introduced to the SHRAD system under the initial control structure, and the corresponding dynamic responses of product purity and sensitive stage temperature are shown in Figure 12 and Figure 13. As shown in Figure 12, when the feed flowrate changes, the ethanol purity leans to the set value after a small fluctuation and finally stabilizes at about the 6th hour. The fluctuation trend can also be seen from the dynamic response of the 25th stage temperature. When the feed flowrate increases by 10%, the water purity returns to the set value within 1 h after experiencing a small fluctuation. However, when the feed flowrate decreases by 10%, the water purity continues to fall and finally stabilizes at about 97 wt % after the fluctuation, which is lower than that without the control structure. As shown in Figure 13, when the water composition in the feed increases, the effect on ethanol and water products is very small, but when the water composition in the feed decreases, the purity of ethanol and water shows great fluctuations. For ethanol products, the fluctuation time is nearly 15 h, and water also has a fluctuation time of about 10 h before it is close to stability. The purities of ethanol and water basically returned to their initial value, and the residual difference is very small.

However, the temperature control loop of the benzene recycle column is not effective. In addition, when the water composition in the feed decreases, the purity of the two products and the temperature of the sensitive stage show an obvious fluctuation with a large overshoot, which is unfavorable for the products. Therefore, the initial control structure needs to be improved.

https://doi.org/10.1021/acsomega.2c00478
ACS Omega 2022, 7, 11382−11394

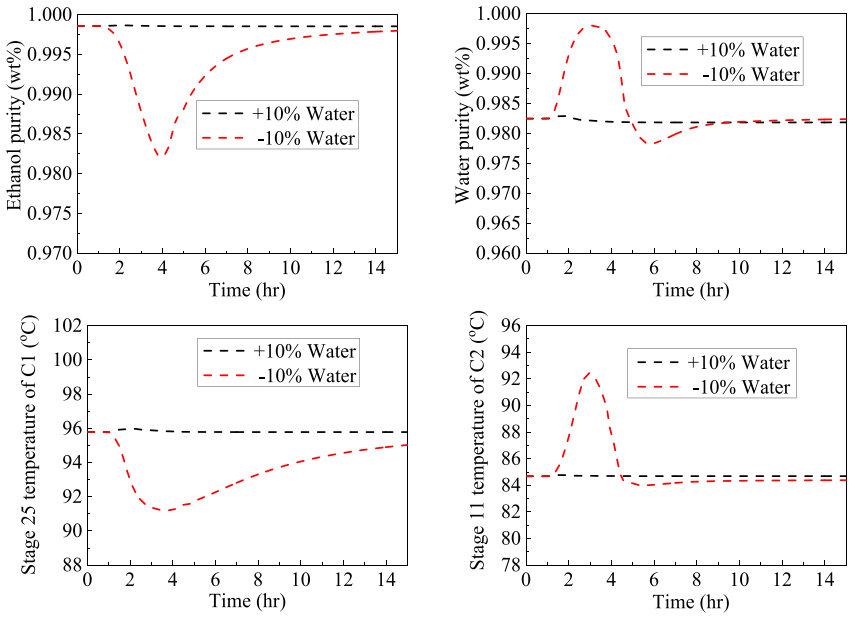

Figure 13. Dynamic responses of the initial control structure in ±10% water composition changes.

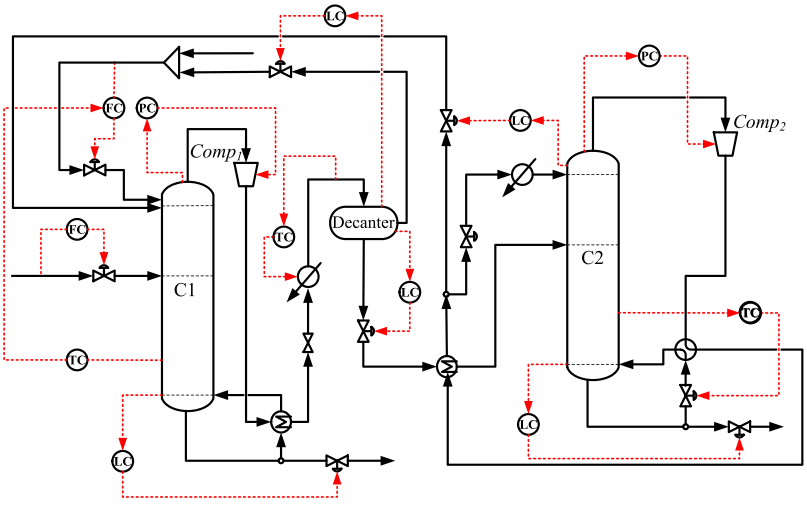

Figure 14. Improved control structure of the SHRAD process.

In this initial control structure, when the feed flowrate changes, ethanol purity can quickly restore stability with high purity. However, when the water composition changes, especially when the water composition decreases, the stability of ethanol production takes a long time, which may be due to the disturbance to the 25th stage temperature being not sensitive enough. It was found that the ratio control of feed flow to organic flow was not effective to control the SHRAD system. Hence, in the improved control structure, the ratio control is deleted. In addition, the control of the 11th stage temperature in the benzene recovery column is not effective, and the bottom flow of the benzene recovery column is used as the operating variable to adjust the 11th stage temperature (K_C = 1.05, τ_I = 8.37 min). The improved control structure is shown in Figure 14.

Figure 15 and Figure 16 show the dynamic responses of the improved control structure in 10% feed flowrate and water composition changes, respectively. As shown in Figure 15, after the feed flow is changed, the ethanol product can recover to the set value, which is similar to the response results of the initial control structure. After the change in feed flow, water purity can be restored to the set point in a short time, and the overshoot of water is smaller compared with that of the initial control structure. As shown in Figure 16, when water composition changes by 10%, the product purity can meet the requirement, and when the water composition decreases, the overshoot of the two products decreases significantly. The fluctuation time of the ethanol product is about 7 h, which is significantly shorter than that in the initial control structure.

4. CONCLUSIONS

In order to recover the low-temperature heat of the distillation system, the self-heat recuperation technology is applied to the azeotropic distillation for the separation ethanol/water mixture. In this paper, the conventional azeotropic distillation and SHRAD processes are simulated and optimized with the multi-objective genetic algorithm method. According to the calculation results, there is a proper design point in the Pareto front of the SHRAD process, for which the SHRAD system has the lowest TAC, the highest thermodynamic efficiency, and the

https://doi.org/10.1021/acsomega.2c00478
ACS Omega 2022, 7, 11382−11394

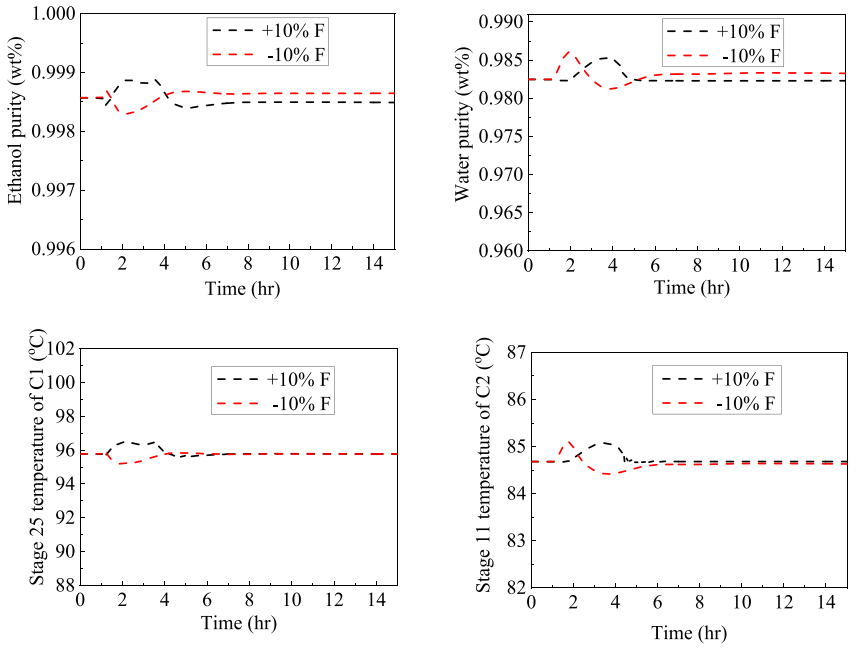

Figure 15. Dynamic responses of the improved control structure in ±10% feed flowrate changes.

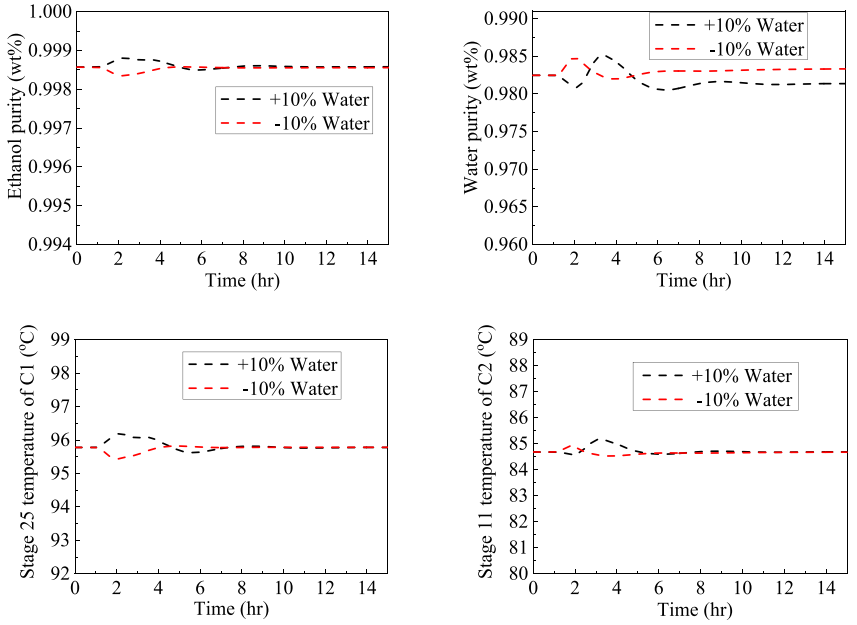

Figure 16. Dynamic responses of the improved control structure in ±10% water composition changes.

least CO_2 emission. Then, the dynamic characteristics of the optimized SHRAD process are analyzed through introducing the feed disturbances, and two control structures are proposed. The ratio control of feed flow to organic phase flow is often used as an operational variable to control the sensitive stage temperature in conventional azeotropic distillation. However, the ratio control is not effective for this SHRAD process. Thus, the initial control structure is improved. The improved control structure can maintain the product purity near the set point with a small overshoot. Although the SHRAD configuration is complex, it can operate effectively with a reasonable control structure. Therefore, the proposed SHRAD process has great potential for the separation of an ethanol/water mixture.

AUTHOR INFORMATION

Corresponding Author

Lumin Li − *School of Resources and Chemical Engineering, Sanming University, Sanming 365004, China;* orcid.org/0000-0002-2803-2392; Phone: +86 17350336271; Email: lilumin1989@163.com

Authors

Na Yu − *Dongying Emergency Management Agency, Dongying 257000, China*

Yi Zhu − *Zhejiang Zhiying Petrochemical Technology Co., Ltd., Hangzhou 310000, China*

Complete contact information is available at: https://pubs.acs.org/10.1021/acsomega.2c00478

https://doi.org/10.1021/acsomega.2c00478
ACS Omega 2022, 7, 11382−11394

Notes

The authors declare no competing financial interest.

■ ACKNOWLEDGMENTS

This work was supported by the Natural Science Foundation of Fujian Province (Grant: 2020J05093), Fujian Province Young and Middle-Aged Teacher Education Research Project (JT180490; JT180492); High-Level Scientific Research Foundation for Sanming University Introduction of Talent (17YG05); National Fund Cultivation Program of Sanming University (PYT2001), and The Research Foundation of Sanming Institute of Fluorochemical Industry (FCIT20171206 and FCIT20171215). Furthermore, the authors are grateful to the editor and the anonymous reviewers.

■ NOMENCLATURE

CAD=conventional azeotropic distillation
C_i=compression ratio of compressor i
$Comp_i$=compressor i
C1=azeotropic distillation column
C2=benzene recovery column
F_{Ben}=flowrate of entrainer benzene
K_C=controller gain
$L_{SP,i}$=the ratio of bottom product flow to the bottom liquid flow of column i
N_i=the number of stages of column i
$N_{F,i}$=feed location of column i
P_{CO2}=emissions of carbon dioxide
SHRAD=self-heat recuperative azeotropic distillation
SHRD=self-heat recuperation distillation
TAC=total annual cost
V_{SP}=the ratio of recycled flow rate to the top steam of the benzene recovery column
W_i=compressor power of column i
η=thermodynamic efficiency
τ_I=controller integral time constant

■ REFERENCES

(1) Haaz, E.; Fozer, D.; Toth, A. J. Development of Anhydrous Ethanol Purification: Reduction of Acetal Content and Vapor−Liquid Equilibrium Study of the Ethanol−Acetal Binary System. *ACS Omega* **2021**, *6*, 1289−1298.
(2) Vane, L. M. Separation Technologies for the Recovery and Dehydration of Alcohols from Fermentation Broths. *Biofuels, Bioprod. Biorefin.* **2008**, *2*, 553−588.
(3) Li, G.; Bai, P. New Operation Strategy for Separation of Ethanol-Water by Extractive Distillation. *Ind. Eng. Chem. Res.* **2012**, *51*, 2723−2729.
(4) Pan, Q.; Shang, X.; Li, J.; Ma, S.; Li, L.; Sun, L. Energy-Efficient Separation Process and Control Scheme for Extractive Distillation of Ethanol-Water Using Deep Eutectic Solvent. *Sep. Purif. Technol.* **2019**, *219*, 113−126.
(5) Zhao, T.; Geng, X.; Qi, P.; Zhu, Z.; Gao, J.; Wang, Y. Optimization of Liquid−Liquid Extraction Combined with Either Heterogeneous Azeotropic Distillation or Extractive Distillation Processes to Reduce Energy Consumption and Carbon Dioxide Emissions. *Chem. Eng. Res. Des.* **2018**, *132*, 399−408.
(6) Cui, Y.; Shi, X.; Guang, C.; Zhang, Z.; Wang, C.; Wang, C. Comparison of Pressure-Swing Distillation and Heterogeneous Azeotropic Distillation for Recovering Benzene and Isopropanol from Wastewater. *Process Saf. Environ. Prot.* **2019**, *122*, 1−12.
(7) Kianinia, M.; Abdoli, S. M. The Design and Optimization of Extractive Distillation for Separating the Acetone/n-Heptane Binary Azeotrope Mixture. *ACS Omega* **2021**, *6*, 22447−22453.
(8) He, S.; Fan, W.; Huang, H.; Gao, J.; Xu, D.; Ma, Y.; Wang, Y. Separation of the Azeotropic Mixture Methanol and Toluene Using Extractive Distillation: Entrainer Determination, Vapor−Liquid Equilibrium Measurement, and Modeling. *ACS Omega* **2021**, *6*, 34736−34743.
(9) Mtogo, J. W.; Toth, A. J.; Szanyi, A.; Mizsey, P. Comparison of Controllability Features of Extractive and Pressure Swing Distillations on the Example of Tetrahydrofuran Dewatering. *ACS Omega* **2021**, *6*, 35355−35362.
(10) Timoshenko, A. V.; Anokhina, E. A.; Morgunov, A. V.; Rudakov, D. G. Application of the Partially Thermally Coupled Distillation Flowsheets for the Extractive Distillation of Ternary Azeotropic Mixtures. *Chem. Eng. Res. Des.* **2015**, *104*, 139−155.
(11) Shan, B.; Niu, C.; Meng, D.; Zhao, Q.; Ma, Y.; Wang, Y.; Zhu, Z. Control of the Azeotropic Distillation Process for Separation of Acetonitrile and Water with and without Heat Integration. *Chem. Eng. Process.* **2021**, *165*, No. 108451.
(12) Ponce, G. H. S. F.; Alves, M.; Miranda, J. C.; Maciel Filho, R.; Maciel, M. R. W. Using An Internally Heat-Integrated Distillation Column for Ethanol-Water Separation for Fuel Applications. *Chem. Eng. Res. Des.* **2015**, *95*, 55−63.
(13) Cong, H.; Li, X.; Li, H.; Murphy, J. P.; Gao, X. Performance Analysis and Structural Optimization of Multi-Tube Type Heat Integrated Distillation Column (HIDiC). *Sep. Purif. Technol.* **2017**, *188*, 303−315.
(14) Dejanović, I.; Matijašević, L.; Olujić, Ž. Dividing Wall Column-A Breakthrough Towards Sustainable Distilling. *Chem. Eng. Process.* **2010**, *49*, 559−580.
(15) Asprion, N.; Kaibel, G. Dividing Wall Columns: Fundamentals and Recent Advances. *Chem. Eng. Process.* **2010**, *49*, 139−146.
(16) Maleta, V. N.; Kiss, A. A.; Taran, V. M.; Maleta, B. V. Understanding Process Intensification in Cyclic Distillation Systems. *Chem. Eng. Process.* **2011**, *50*, 655−664.
(17) Chen, J.; Ye, Q.; Liu, T.; Xia, H.; Feng, S. Improving the Performance of Heterogeneous Azeotropic Distillation via Self-Heat Recuperation Technology. *Chem. Eng. Res. Des.* **2019**, *141*, 516−528.
(18) Long, N. V. D.; Lee, M. A Novel Self-Heat Recuperative Dividing Wall Column to Maximize Energy Efficiency and Column Throughput in Retrofitting and Debottlenecking of A Side Stream Column. *Appl. Energy* **2015**, *159*, 28−38.
(19) Kansha, Y.; Kishimoto, A.; Nakagawa, T.; Tsutsumi, A. A Novel Cryogenic Air Separation Process Based on Self-Heat Recuperation. *Sep. Purif. Technol.* **2011**, *77*, 389−396.
(20) Kansha, Y.; Kishimoto, A.; Tsutsumi, A. Application of the Self-Heat Recuperation Technology to Crude Oil Distillation. *Appl. Therm. Eng.* **2012**, *43*, 153−157.
(21) Long, N. V. D.; LEE, M. A Novel NGL (Natural Gas Liquid) Recovery Process Based on Self-Heat Recuperation. *Energy* **2013**, *57*, 663−670.
(22) Alcántara-Avila, J. R.; Kano, M.; Hasebe, S. Multiobjective Optimization for Synthesizing Compressor-Aided Distillation Sequences with Heat Integration. *Ind. Eng. Chem. Res.* **2012**, *51*, 5911−5921.
(23) Ryan, P. J.; Doherty, M. F. Design/Optimization of Ternary Heterogeneous Azeotropic Distillation Sequences. *AIChE J.* **1989**, *35*, 1592−1601.
(24) Luyben, W. L. Economic Optimum Design of the Heterogeneous Azeotropic Dehydration of Ethanol. *Ind. Eng. Chem. Res.* **2012**, *51*, 16427−16432.
(25) Luyben, W. L. Control of A Multiunit Heterogeneous Azeotropic Distillation Process. *AIChE J.* **2006**, *52*, 623−637.
(26) Kiss, A. A.; David, J.; Suszwalak, P. C. Enhanced Bioethanol Dehydration by Extractive and Azeotropic Distillation in Dividing-Wall Columns. *Sep. Purif. Technol.* **2012**, *86*, 70−78.
(27) Sun, L. Y.; Chang, X. W.; Qi, C. X.; Li, Q. S. Implementation of Ethanol Dehydration Using Dividing-Wall Heterogeneous Azeotropic Distillation Column. *Sep. Sci. Technol.* **2011**, *46*, 1365−1375.
(28) Li, Y.; Xia, M.; Li, W.; Luo, J.; Zhong, L.; Huang, S.; Ma, J.; Xu, C. Process Assessment of Heterogeneous Azeotropic Dividing-Wall

https://doi.org/10.1021/acsomega.2c00478
ACS Omega 2022, 7, 11382−11394

Column for Ethanol Dehydration with Cyclohexane as An Entrainer: Design and Control. *Ind. Eng. Chem. Res.* **2016**, *55*, 8784−8801.
(29) Gomis, V.; Pedraza, R.; Francés, O.; Font, A.; Asensi, J. C. Dehydration of Ethanol Using Azeotropic Distillation with Isooctane. *Ind. Eng. Chem. Res.* **2007**, *46*, 4572−4576.
(30) Kansha, Y.; Tsuru, N.; Fushimi, C.; Tsutsumi, A. New Design Methodology Based on Self-Heat Recuperation for Production by Azeotropic Distillation. *Energy Fuel.* **2010**, *24*, 6099−6102.
(31) Li, J.; Li, L.; Li, R.; Yang, Z.; Ma, Z.; Sun, L.; Zhang, N. Investigation of Multi-Objective Optimization for Integrating Design and Control of Ionic Liquid-Based Extractive Distillation. *Chem. Eng. Res. Des.* **2021**, *170*, 134−146.
(32) Parhi, S. S.; Rangaiah, G. P.; Jana, A. K. Multi-Objective Optimization of Vapor Recompressed Distillation Column in Batch Processing: Improving Energy and Cost Savings. *Appl. Therm. Eng.* **2019**, *150*, 1273−1296.
(33) Olujić, Ž.; Sun, L.; De Rijke, A.; Jansens, P. J. Conceptual Design of An Internally Heat Integrated Propylene-Propane Splitter. *Energy* **2006**, *31*, 3083−3096.
(34) Douglas, J. M. *Conceptual Design of Chemical Processes*; McGraw-Hill: New York, 1988.
(35) Seider, W. D.; Seader, J. D.; Lewin, D. R. *Product & Process Design Principles: Synthesis, Analysis and Evaluation*; John Wiley & Sons: 2009.
(36) Gadalla, M. A.; Olujic, Z.; Jansens, P. J.; Jobson, M.; Smith, R. Reducing CO_2 Emissions and Energy Consumption of Heat-Integrated Distillation Systems. *Environ. Sci. Technol.* **2005**, *39*, 6860−6870.
(37) Li, L.; Tu, Y.; Sun, L.; Hou, Y.; Zhu, M.; Guo, L.; Li, Q.; Tian, Y. Enhanced Efficient Extractive Distillation by Combining Heat-Integrated Technology and Intermediate Heating. *Ind. Eng. Chem. Res.* **2016**, *55*, 8837−8847.
(38) Luyben, W. L. *Distillation Design and Control Using Aspen Simulation*. John Wiley & Sons, 2013, DOI: 10.1002/9781118510193.
(39) Luyben, W. L.; Chien, I. L. *Design and Control of Distillation Systems for Separating Azeotropes*; John Wiley & Sons: 2010.
(40) Luyben, W. L. Control of An Azeotropic DWC with Vapor Recompression. *Chem. Eng. Process.* **2016**, *109*, 114−124.

https://doi.org/10.1021/acsomega.2c00478
ACS Omega 2022, 7, 11382−11394